Since January 2020 Elsevier has created a COVID-19 resource centre with free information in English and Mandarin on the novel coronavirus COVID-19. The COVID-19 resource centre is hosted on Elsevier Connect, the company's public news and information website.

Journal of Photochemistry & Photobiology, B: Biology 234 (2022) 112538

Contents lists available at ScienceDirect

Journal of Photochemistry & Photobiology, B: Biology

journal homepage: www.elsevier.com/locate/jphotobiol

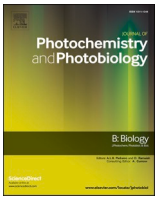

Questioning ZnO, Ag, and Ag/ZnO nanoparticles as antimicrobial agents for textiles: Do they guarantee total protection against bacteria and SARS-CoV-2?

Daniel J. da Silva [a], Adriana Duran [a], Aline D. Cabral [a], Fernando L.A. Fonseca [b], Rodrigo F. Bueno [c], Derval S. Rosa [a,*]

[a] Center for Engineering, Modeling, and Applied Social Sciences (CECS), Federal University of ABC (UFABC), Santo André, Brazil
[b] Faculty of Medicine of ABC (FMABC), Department of Clinical Analysis, Santo André, São Paulo, Brazil
[c] Coordinator of the COVID-19 Monitoring Network in Wastewater National Water and Basic Sanitation Agency, Ministry of Science, Technology and Innovation and Ministry of Health, Center for Engineering, Modeling, and Applied Social Sciences (CECS), Federal University of ABC (UFABC), Santo André, Brazil

ARTICLE INFO

Keywords:
SARS-CoV-2
Antimicrobial
ZnO
Silver
Multifunctional textiles

ABSTRACT

Coronavirus Disease 2019 (COVID-19) occasioned global economic and health systems collapse. Also, it raised several concerns about using conventional cotton fabrics for manufacturing personal protective equipment without the antimicrobial capacity to inactivate viruses, such as Severe Acute Respiratory Syndrome Coronavirus 2 (SARS-CoV-2) and its variants. Therefore, developing antimicrobial cotton fibers is crucial to avoid new global pandemics or the transmission of dangerous pathogens that remain on surfaces for long periods, especially in hospitals and medical clinics. Herein, we developed antimicrobial cotton fabrics with Ag, ZnO, and Ag/ZnO nanoparticles and evaluated their bactericidal activity against *Escherichia coli* (*E. coli*) and *Staphylococcus aureus* (*S. aureus*), photocatalytic activity, and antiviral activity against Delta SARS-CoV-2. Although the antimicrobial fabrics are effective against these bacteria, they only reduce part of the SARS-CoV-2 virions during the first 15 min of direct contact via damage only to biological structures on the viral surface particle while the viral RNA remains intact.

1. Introduction

With the current global pandemic of Coronavirus Disease 2019 (COVID-19) caused by Severe Acute Respiratory Syndrome Coronavirus 2 (SARS-CoV-2) [1], several efforts are being made to develop functional materials with the ability to disable this coronavirus quickly [2]. This preoccupation occurs since SARS-CoV-2 can remain infectious on the surface of various materials used as personal protective equipment (PPE) and clothes for more than one day [3–7]. Recently, Virtanen et al. [8] reported that SARS-CoV-2 could remain infectious on contaminated clothing materials for up to 5 days, bringing several concerns about human safety.

Humans have widely used cotton fibers as a renewability and biodegradability feedstock to manufacture clothes essential for the maintenance of human life [9]. Cotton fabrics (CF) do not have an intrinsic antimicrobial capacity, requiring surface treatments of this natural material mainly to produce safe biological PPEs, such as masks and coats. ZnO and silver have been the leading industrial and scientific options for this purpose, showing inhibiting effectiveness against the growth of a broad spectrum of pathogenic microorganisms [10–13]. They are widely used as intrinsic antimicrobial agents due to their ability to cause the death of microorganisms and the destruction of the viral structure by metal ions releasing and reactive oxygen species (ROS) generation.

ZnO is a semiconductor metallic oxide, non-toxic, low-cost, considered safe for direct contact with humans and animals, being a versatile material to be designed in several nanostructures [14]. ZnO displays have been explored in different technological areas due its photocatalytic properties, such as photocatalysis, photoelectronic, sensor, and photovoltaic cells [15]. Silver is a noble metal with a well-established antimicrobial activity and can improve the photocatalytic performance of semiconducting oxides via plasmon resonance, which induces electron transfer at silver/oxide interfacial, occasioning a delay on recombination electron-hole pairs [16]. Several methods have been

* Corresponding author at: Av. dos Estados, 5001. CEP 09210-210 Santo André, SP, Brazil.
E-mail address: dervalrosa@yahoo.com.br (D.S. Rosa).

https://doi.org/10.1016/j.jphotobiol.2022.112538
Received 25 January 2022; Received in revised form 24 July 2022; Accepted 1 August 2022
Available online 4 August 2022

utilized to synthesize nanoparticles (NPs) of these materials [17–19]. Among them, sonosynthesis is an emerging route adequate to prepare NPs in a sustainable and no-time-consuming way [20–24]. For his purpose, ZnO and silver nanoparticles (NPs) are prepared by submitting their precursors to ultrasonic irradiation that cause acoustic cavitation, local heating (superior to 5000 K), and local pressurization (higher than 1000 atm). Using these antimicrobial agents as nanoparticles with diameters lesser than 100 nm brings advantages for antimicrobial applications, such as high surface area and the possibility of using a low amount of material, mainly for silver, an expensive metal.

In this contribution, we successfully synthesized AgNPs, ZnO-NPs, and AgNPs, ZnO-NPs, and their nanocomposites via sonochemistry. Moreover, we effectively fixed these nanoparticles on the CF surface. Our findings show that these nanoparticles may not provide sufficient antimicrobial capacity for cotton fabrics (CF) to ensure rapid and effective protection against infectious SARS-CoV-2 particles, which is worrisome since several coronavirus variants are emerging worldwide.

2. Materials and methods

2.1. Materials

The cotton fabrics (CF) were purchased from a local fabric store (São Paulo, Brazil). ZnO-NPs (< 50 nm) were acquired from Sigma-Aldrich Inc. (São Paulo, Brazil). Anhydrous gallic acid was obtained from InLab. Phenol, neutral detergent, ethanol, L-ascorbic acid, trisodium citrate, and silver nitrate were obtained from Labsynth (São Paulo, Brazil). The water-based acrylic binder (Acrylic Resin 180 W) was purchased from Redelease (São Paulo, Brazil). Nutrient agar culture medium was purchased from Himedia. Methylene blue (MB) was acquired from Merck.

2.2. Synthesis of AgNPs and Ag/ZnO-NPs

Trisodium citrate (1 g) was dissolved in 100 mL of ZnO aqueous suspensions (0, 1000, and 2000 ppm) and $AgNO_3$ in different concentrations (0, 500, and 1000 ppm). Then the suspension was ultrasonicated for 3 min, using a tip ultrasound (Vibra Cell VCX 500, Sonics, USA), with an amplitude of 40%.

2.3. Coating Procedure

The binder (1 g) was mixed with the NPs suspension (100 mL). Then, cotton fabric (with a dimension of 10 cm × 10 cm and prewashed with aqueous detergent solution, 6.7 g L^{-1}) was immersed in this bath and left for 30 min. After that, the cotton fabric was heated at 120 ± 5 °C (20 min), washed and dried at 120 ± 5 °C (20 min). The coated cotton fabrics (CF) were named ZnO(*Y*ppm) + Ag(*X*ppm), where *Y* and *X* represent the concentration of ZnO and silver ions applied in the NPs liquor.

2.4. Characterization of the Nanoparticles

The particle diameter distribution was recorded using the dynamic light scattering (DLS) technique with a 90° scattering angle. Zetasizer Nano-ZS (Malvern Panalytical Ltd., Malvern, U.K.) was the equipment utilized for the DLS characterization. Aliquots of the suspensions (100 μL) were suspended in distilled water (2 mL), and each sample was analyzed in triplicate. The Zeta potential (ζ) was estimated by the Smoluchowski modeling of the electrophoretic mobility of the nanoparticles measured by Zetasizer Nano-ZS (Malvern Instruments). The reading time to obtain the zeta potential data was 10 s, and the measurements were performed in triplicate. The absorption spectra from the aqueous nanoparticle suspensions with the synthesized nanoparticles were collected by UV–vis spectrophotometer (Varian Cary Model 50) at the 200–800 nm wavelength. The optical bandgap (E_g) of the nanoparticles was obtained from the UV–Vis spectra using the graphical method: plotting $(\alpha h\nu)^{1/n}$ versus $h\nu$ and extrapolating the linear region on the radiation energy axis ($h\nu$). h is Planck's constant, ν is the frequency of electromagnetic radiation, n depends on the nature of the transition (n equal to 2 for indirect transition and equal to ½ for direct transition), and α is the absorption coefficient.

2.5. Characterization of the Coated Cotton Fabrics

Scanning electron microscopy (SEM) and energy-dispersive X-ray spectroscopy (EDS) were performed in the JEOL JSM-6010LA scanning electron microscope equipped with a chemical microanalysis module (EDS), using a working distance of 14 mm and an electron acceleration voltage of 10 keV. The samples were previously coated with a 20 nm thick gold layer, using Sputtering Leica EM ACE 200 (Leica Microsystems, São Paulo, Brazil). Fourier-transform infrared spectroscopy (FTIR) with attenuated total reflectance (ATR) diamond accessory was performed on Frontier 94,942 equipment (PerkinElmer Inc., Massachusetts, USA). The spectra were collected with 4 cm^{-1} spectral resolution, 64 scans, from 4000 to 600 cm^{-1}. The photocatalytic activity was evaluated by monitoring the photodecomposition of methylene blue (MB) under blue light irradiation (2.8 eV). The cotton fabrics (1 cm × 1 cm) were immersed in 5.75 mL of aqueous solutions of MB (37.5 mg mL^{-1}, pH = 7). To start the photocatalytic reactions, the solutions with the samples were exposed to constant illumination of a blue lamp (100 W). Then, the solution was analyzed at regular intervals using a UV–Vis spectrophotometer (UV-M51, LAB 1000) by measuring the absorption at 665 nm. The photodegradation efficiency (*e*) against methylene blue (MB) was calculated by Eq. (1).

$$e\ (\%) = 100 \times \frac{A_0 - A_t}{A_0} \tag{1}$$

where A_0 is the initial absorbance of MB solution; A_t is the absorbance of the MB solution after illumination at time t.

Agar diffusion assays were performed as bactericidal tests by placing samples (1 cm × 1 cm) in contact with the sterilized Petri dishes with nutrient agar culture medium and inoculated with bacteria suspension (*Escherichia coli*, *E. coli* ATCC 25922, or *Staphylococcus aureus, S. aureus* ATCC 6548) at 10^5 CFU mL^{-1}. The samples were incubated at 36 ± 1 °C and 85% humidity. The inoculums viability was confirmed via a spread-plate method on agar nutrient as the positive control. The inhibition zone from the biocidal activity of the multifunctional fabrics was evaluated after 48 h of incubation. ROS active species generated by the CF coated with NPs were evaluated by the photodegradation of MB using trapping agents (1 mmol/L): phenol, ethanol, and L-ascorbic acid were added to the MB photodegradation to catch hydroxyl radical (OH*), holes (h^+), hydroperoxyl radical (HO_2*), respectively. Gallic acid was utilized as a simultaneous trapping agent for OH*, HO_2*, and hydrogen peroxide (H_2O_2). The trapping experiment was identical to the photocatalytic degradation assay of MB except that was added the radical scavengers in the system. The photocatalytic activity was estimated by the pseudo-first-order kinetic model (Eq. 2) from the Langmuir-Hinshelwood model.

$$ln\left(\frac{C_t}{C_0}\right) = -kt \tag{2}$$

where C_0 is the initial concentration of MB solution; C_t is the MB concentration in the solution after illumination at time t; k is the rate constant of the photocatalytic reaction (min^{-1}). The relative concentration (C_t/C_0) was calculated by the relative absorbance (A_t/A_0).

2.6. SARS-CoV-2 Tests

SARS-CoV-2 infected oropharyngeal and nasopharyngeal swabs (sterile swabs) were collected from patients (anonymous – unidentified)

diagnosed with COVID-19. The patients were contaminated with the Delta SARS-CoV-2 variant. The Delta strain was identified by genetic sequencing with Nanopore's MinION sequencer, using the ARTIC protocol. The swabs were placed in sterile saline solution (NaCl, 0.9%) in Falcon tubes (approximately 5 mL) and frozen at −20 °C until processing. Five biological samples were selected, with a Ct value between 16 and 20 (RT-qPCR previously performed for diagnosis, in the FMABC laboratory) as a parameter used for selection, and these samples were used to form a sample "mix" in order to increase the amount (in mL). To assess the antiviral efficiency of the cotton fabrics, three exposure times were selected: 5, 10, and 15 min. We put 50 μL of the sample "mix" ($COVID^+$) in each Eppendorf tube with the respective CF (10 variations, as previously established) at room temperature and wait for the incubation period. After the incubation period, we added 300 μL of lysis solution for virus inactivation (Lysis Buffer – PureLink Invitrogen kit). These samples submitted to the incubation process with the fabrics were applied on antigen-detecting rapid test and quantitative reverse transcription-polymerase chain reaction (RT-qPCR) for SARS-CoV-2. SARS-CoV-2 Rapid Antigen Test kit (Roche) (reference 9901-ncov-01 g) was applied to detect the presence of antigens in the samples studied [25]. Three drops of the sample "mix" were placed in the place indicated on the cassette using the "accessories" that make up the kit to visualize, following the manufacturer guide. The rapid tests are chromatographic immunoassays for the qualitative detection of specific SARS-CoV-2 antigens. Then, the reduction of the number of infectious viruses on the media (antiviral activity) was estimated by the red and white color intensity of the "test line" in rapid diagnostic tests using ImageJ software. The antigen detection limits of rapid tests for SARS-CoV-2 are: Quantity of stock of the titrant in the tests is: $1 \times 10^{6.2}$ $TCID_{50}$/mL (maximum red intensity); Minimum detected viral load is $3.12 \times 10^{2.2}$ $TCID_{50}$/mL (maximum white color intensity). The red and white color intensities were normalized to estimate the antigen $TCID_{50}$/mL percentual reduction from rapid tests. The SARS-CoV-2 inoculum (frozen and stored at −20 °C) was vortexed for 30 s after defrosting. Then, the extraction process was started in a commercial kit (PureLink™ Viral RNA Mini Kit - Invitrogen™) using 350 μL of ethanol (70%) and homogenization. Next, 700 μL of the sample was transferred to the column and centrifuged for 1 min at 12,00 rpm, discarding the flow-through. The next step was washing with 700 μL of Wash Buffer I. Centrifugation for 1 min at 12,000 rpm. Discard the flow-through. 500 μL of Wash Buffer II was added. Centrifugation for 1 min at 12,000 rpm and this procedure was repeated, washing the sample twice with this same buffer. After the second wash, the filtrate was discarded, and centrifugation was carried out for 2 min at 12,000 rpm with the column dry. The column was transferred to a 1.5 mL microtube, and 50 μL of ultrapure water was added; the sample was then incubated for 1 min at room temperature and centrifuged for 2 min at 12,000 rpm. RNA was stored at −80 °C until detection of SARS-CoV-2 by RT-qPCR. Verification of the presence of SARS-CoV-2 genetic material was performed by PCR assays using the 2019-nCoV TaqMan RT-PCR kit (Norgen, Cat. TM67120). Manufacturers' guidelines were followed to operate the kit and the equipment used (CFX Opus Real-Time PCR Systems – Bio-Rad). The mix for the reactions was planned to reach a final volume of 20 μL, using in its composition: 5 μL of extracted RNA, 10 μL of Master Mix 2×, 1.5 μL of Mix (Primer and Probe in amounts proportional to those indicated for the assay) and 3.5 μL of ultrapure water, always in duplicate samples. The programmed reaction cycle was: cycle 1–50 °C for 30 min; cycle 2–95 °C for 3 min; cycle 3–45 × 95 °C for 3 s and 55 °C for 30 s. A negative control (water + reaction mix) and a set of positive controls in serial dilution (10^4, 10^5, 10^6, 10^7) we used to compose a standard curve for the selected targets (genes N1 and N2). Calibration curve data: N1 ($y = -3.491\times + 43.065$; $R^2 = 0.996$; Efficiency = 93.4%), N2 ($y = -3.723\ x + 44.750$; $R^2 = 0.998$; Efficiency = 85.6%) The limit of detection (LOD) was 10 copies of the genome for: Ct of 39.28 ± 0.05 for N1 and Ct of 39.77 ± 0.58 for N2. The antiviral activity (percentual reduction of the number of infectious SARS-CoV-2 particles) on the infected media was estimated by the color intensity of the "test line" in rapid diagnostic tests (Fig. 6S) using ImageJ software.

2.7. Statistical Analyses

Analysis of variance (ANOVA one-way) and Tukey's test (*t*-test) were applied to statistically evaluate the significant differences between the samples' measured SARS-CoV-2 antiviral data using the GraphPad Prism 7 and a 95% confidence level. Response surface and randomized factorial experimental designs for the color map fitting and Pareto charts of the inhibition zone diameter determined from the bacterial plaque assay against *E. coli* and *S. aureus*, rate constant (k), direct optical bandgap (E_g^d) and indirect optical bandgap (E_g^i) were realized by polynomial surface and randomized factorial models via ANOVA by Fisher's test (F-test) and *t*-test, using Design-Expert v11 (StatEase®) and a 95% confidence level.

3. Results and Discussion

3.1. Nanoparticles

AgNPs, ZnO-NPs, and Ag/ZnO-NPs suspensions were prepared via a sonochemical approach and utilized to address the lack of antimicrobial activity of the CF. The nanoparticles were fixed on the surface of cotton fibers using an acrylic binder to guarantee self-disinfecting activity for the cotton textile. The AgNPs suspension prepared by the reduction of $AgNO_3$ with trisodium citrate and ultrasound irradiation present bimodal hydrodynamic diameter distribution (Fig. 1a), with hydrodynamic diameters (D_H) lesser than 30 nm, but they tend to agglomerate in microparticles of silver with D_H of 1 to 8 μm as indicated by the Zeta potential (ζ) between ±15 mV [26]. The ζ and D_H results are detailed in Table 1S (Supplementary material). The usage of 1000 ppm of silver ions favors the formation of AgNPs with smaller diameters than that obtained by using a concentration of 500 ppm in the sonochemical approach whose the ultrasound waves correspond to the energy source required to initiate the reduction of silver ions (Ag^+) to metallic silver (Ag^0) by the reductant agent [27,28]. ZnO-NPs present D_H of 0.9 ± 0.5 nm that agglomerate in the aqueous suspension ($\zeta = -9.1 \pm 3.5$) like aggregates with 35.5 ± 8.5 nm. Ag/ZnO-NPs were prepared by the sonochemical treatment of previous ZnO-NPs and seem to present electrostatic charges (ζ is within the range of ±30 mV) that avoid their agglomeration in the suspension since the charges make their repelling each other. Ag/ZnO microaggregates also are generated in the suspension when it is used >500 ppm of silver ions or 1000 ppm of ZnO-NPs in the sonochemical synthesis of the Ag/ZnO-NPs. According to ζ potential, these aggregates can be Ag/ZnO microparticles since the Ag/ZnO-NPs suspension present moderate stability with ζ out the range of ±30 mV, except when it is used 2000 ppm and 500 ppm of ZnO-NPs and $AgNO_3$, respectively.

The optical bandgaps of the ZnO-NPs and Ag/ZnO-NPs are displayed in Fig. 1b and 1c as color maps. They were determined by the Tauc plot (Fig. 1S). The direct optical bandgap (E_g^d) of the ZnO-NPs is 3.02 eV following the literature data [29], and it is reduced or values lesser than 2 eV by the modification with silver. The indirect optical bandgap (E_g^i) of the ZnO-NPs are lesser than ultrathin ZnO nanowires hexagonal and wurtzite structures [11], lesser than 1 eV. The modification of the ZnO-NPs with 500 ppm of silver carry to the lowest E_g^i (0.36 eV). The reduction of the $E_g^d$of ZnO-NPs (E_g^d redshift) by Ag occurs due to the surface plasmon effect involving noble metals attached on the surface of the oxides, leading to the injection of electrons from the metal to the oxide [16] by local reversible oxidation reactions of metallic silver (Ag^0) to silver ions (Ag^+). Moreover, Ag also increases the half-life of the excited electrons and electronic holes generated on the surface of the ZnO after absorbing electromagnetic radiation [30], which is suitable to upgrade the ZnO-NPs acting for photocatalytic, antimicrobial, and photovoltaic requirements [16]. Although ZnO is predominantly a direct bandgap semiconductor, ZnO nanostructures have a peculiar characteristic associated with indirect-to-direct and indirect-to-direct bandgap

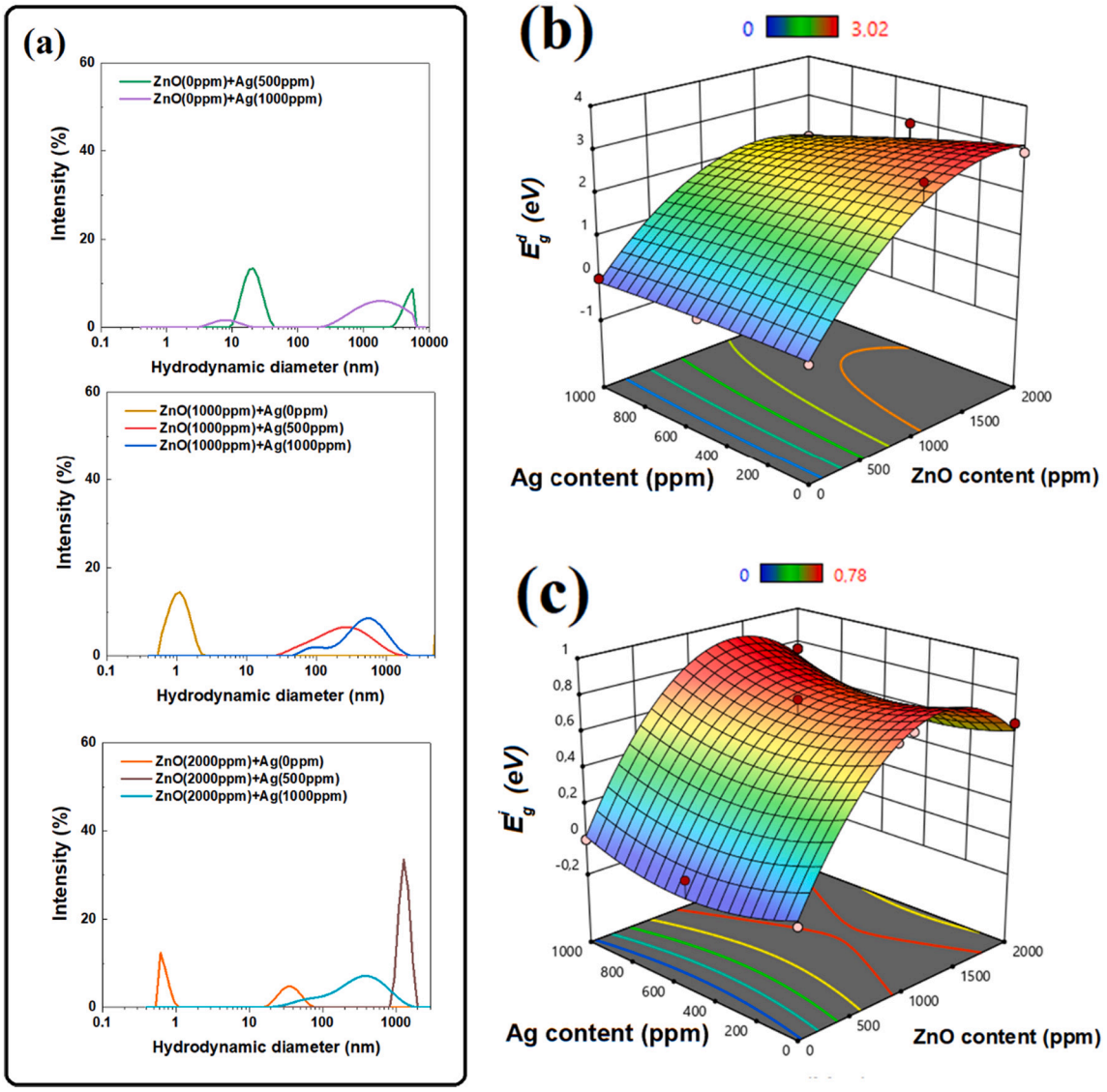

Fig. 1. (a) The hydrodynamic diameter of the AgNPs, ZnO-NPs, and Ag/ZnO-NPs. Color map for the (b) direct optical bandgap (E_g^d) and (c) indirect optical bandgap (E_g^i) of the ZnO-NPs, and Ag/ZnO-NPs after the sonochemical procedure. Adjust error (R^2) higher than 0.96 or the polynomial surface fitting.

transitions occasioned by mechanical strains that change the semiconductor electronic bands. Consequently, the ZnO predominant electronic behavior is modified [31]. The randomized factorial ANOVA (Fig. 2S) shows that only the ZnO content increases in a significant way the direct optical bandgap, while Ag content and interactions between the concentration of these antimicrobial agents have a negligible effect on E_g^d and E_g^i values of the nanoparticles.

3.2. Coated Fabrics

The CF fibers display several spikes (Fig. 2), which may be formed due to the partial solubilization of cellulose on the surface of the fibers during the bleaching treatment applied to cotton textiles using NaOH. This procedure is known as mercerization, which causes surface roughness to increase [32]. The surface coating leads to the modification of the CF surface with AgNPs, as indicated by the contrast changes of the SEM micrographs. However, the magnification limit of the SEM microscope did not allow the detection of the AgNPs on the surface. Also, the cotton fibers, even covered with gold, could not support the electron beam, decomposing if they used larger magnifications or high acceleration voltages (> 10 kV). CF modified with 1000 ppm the ZnO-NPs present the regions covered by the binder used to fix the nanoparticles on the surface of the CF. When 2000 ppm of ZnO-NPs are used, the surface of the fibers is also modified, and the spectra obtained by energy-dispersive X-ray spectroscopy (EDS) (Fig. 3S) show the presence of Zn (0.89 and 1.02 keV). This EDS signal confirms the presence of ZnO-NPs on the CF surface after surface modification. In addition, EDS spectra confirm the presence of silver (in ppm) on the surface of the fabrics coated with AgNPs (Table 2S). Also, it was identified the elements C (0.26 keV) and O (0.53 keV), associated with the chemical composition of cotton with cellulose (predominantly), lignin, and hemicellulose as indicated by the infrared absorption spectra obtained by Fourier-transform infrared spectroscopy (FTIR) (Fig. 4S). The characteristic infrared signals of the fabrics are detailed in Table 3S. The reduction of the IR intensity signals in the range of 980–1070 cm^{-1} (vibrations of C—O chemical bonds of the cellulose) and 3400–3000 cm^{-1} (OH groups from cellulose and adsorbed water) confirms the EDS data, which evidence the effective fixation of the NPs on the fabric surface [33].

Only after surface coating, the CF shows antimicrobial properties against `E. coli` (Gram-negative bacteria) and `S. aureus` (Gram-positive bacteria), as shown in figs. 5S and 6S (Supplementary Material). CF with AgNPs presents only bactericidal effect against `E. coli`, indicating

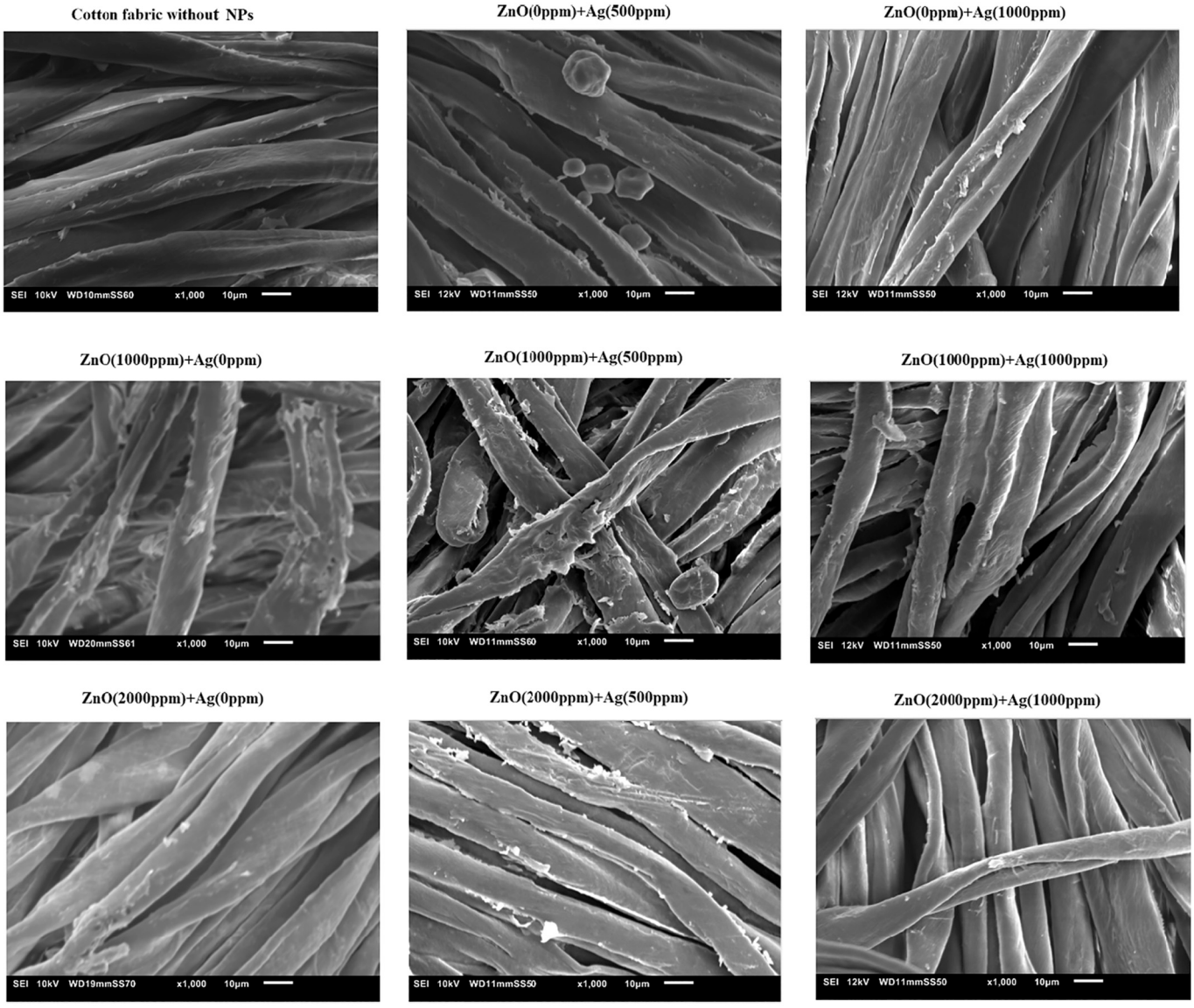

Fig. 2. SEM images of the CF before and after surface modification with different concentrations of Ag, ZnO, and Ag/ZnO nanoparticles.

that the concentration of AgNPs fixed on the CF is not enough to form an inhibition zone against *S. aureus*, hampering these Gram-positive bacteria proliferation by Ag^+ releasing or oxidative stress via reactive oxygen species ROS generation is combined with interactions of silver ions with transport proteins and interference in transcription or replication of DNA. Ag^+ ions cause a non-oxidative bactericidal mechanism involving irreversible damage on bacteria cells by electrostatic attraction of Ag^+ ions with negatively charged microbial membranes [19]. At the same time, ROS ($*O_2^-$, H_2O_2, $^1O_2$, HO_2*, and *OH) disrupts bacteria cell membrane by oxidative stress that destroys biological molecules (proteins, lipids, DNA, and RNA) [34,35].

The combination of ZnO and silver leads to a more pronounced effect against the bacteria of the CF (Fig. 3a and 3b). The color map in Fig. 3b shows clearly that the increase of ZnO or silver in the CF with Ag/ZnO-NPs leads to higher inhibition zone values against *E. coli*. According to the Pareto charts (Fig. 7S), only the ZnO content almost certainly has important effects on inhibition diameter against *S. aureus*. Ag content has no significant effect on the bactericidal performance of the cotton fabrics. AL-Jawad et al. [13] also observed that *S. aureus* (Gram-positive bacteria) seemed to be more resistant to pure and Ag-doped ZnO thin film than *E. coli*. Manna et al. [36] observed that cotton fabrics coated with Ag/ZnO-NPs effectively inhibit the growth of *S. aureus*. Adhikari et al. [37] reported that Ag/ZnO-NPs are more effective in killing *E. coli* than ZnO-NPs under solar irradiation due to the superior photoactivity of these hybridous nanoparticles.

The photocatalytic behavior of the coated CF was evaluated by photodegradation efficiency (*e*) of methylene blue (MB) (Fig. 3c). The CF modified with 500 ppm of Ag, 1000 and 2000 ppm of ZnO-NPs displays the lowest performance for *e*. The color map in Fig. 3d shows that the degradation rate (*k*) is high for the CF with Ag/ZnO-NPs hybrid systems, being more expressive when the NPs are prepared with a mixture of 1000 ppm of both ZnO-NPs and $AgNO_3$. Although it has been shown that Ag/ZnO nanocomposites tend to generate more ROS than pure ZnO-NPs [38], the photodegradation efficiency data evidence that the bactericidal activity of the coated CF is not only associated with photocatalytic mechanism and reduction of the optical bandgap due to the Schottky barrier at the Ag/ZnO interface [39,40]. The metal releasing non-oxidative effect is vital to guarantee a more antimicrobial performance for the CF with Ag/ZnO-NPs since there is a mismatch between the color charts for inhibition zone diameter and *k* data. Manna et al. [36] also verified the best photocatalytic activity for CF coated with Ag/ZnO-NPs against CF with ZnO-NPs, but they did not evaluate

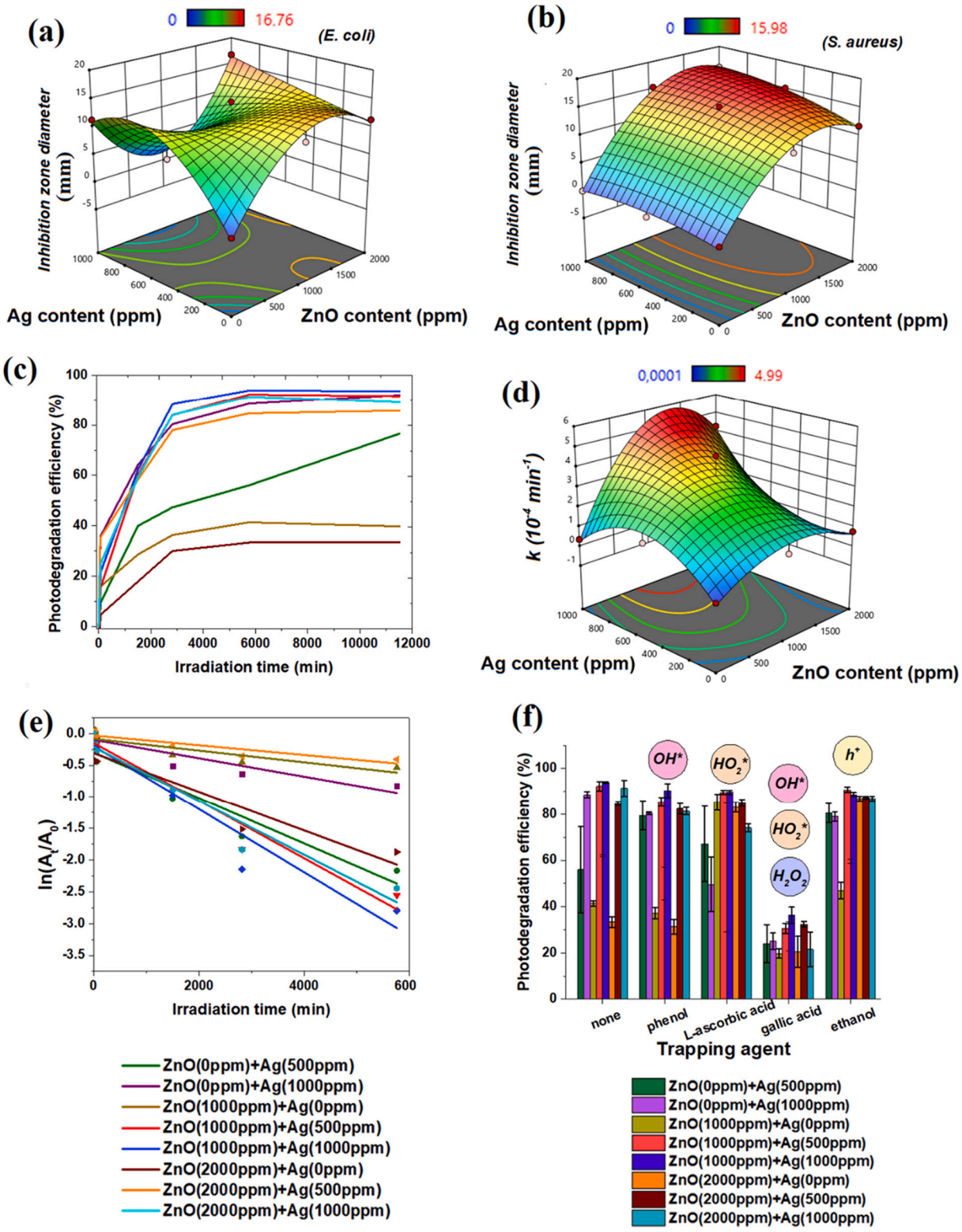

Fig. 3. Color map for the inhibition zone diameter determined from the bacterial plaque assay against *E. coli* (a) and *S. aureus* (b). (c) Photodegradation efficiency of the CF coated with AgNPs, ZnO-NPs, and Ag/ZnO-NPs. (d) Rate constant (k), (e) kinetics profile, and (f) trapping experiment data of the photocatalytic degradation of methylene blue (MB) by the coated CF under blue light irradiation (450 nm). Adjust error (R^2) higher than 0.94 or the polynomial surface fitting. Turkey's test indicates that the ZnO and Ag content significantly influences photodegradation efficiency from trapping experiment data with $p < 0.0001$, using a 95% reliability level. (For interpretation of the references to color in this figure legend, the reader is referred to the web version of this article.)

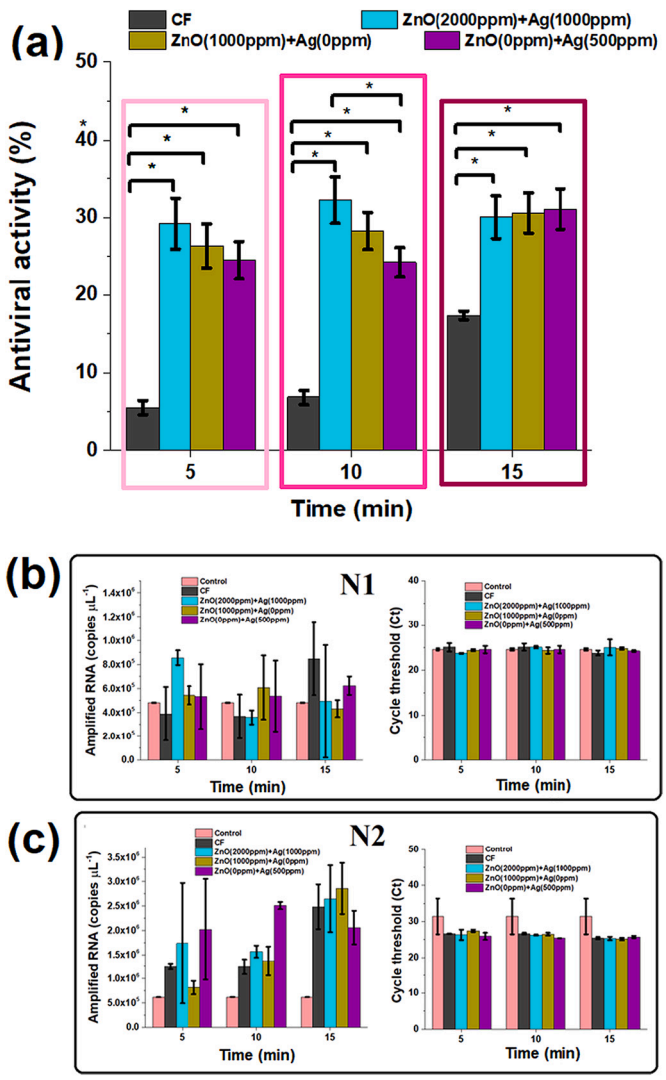

Fig. 4. (a) Antiviral activity of the CF coated with AgNPs, ZnO-NPs, and Ag/ZnO-NPs against SARS-CoV-2 after 5, 10, and 15 min of cotton-virus exposition. Amplified RNA and Ct values determined by RT-qPCR for SARS-CoV-2 using the N1 (b) and N2 (c) gene targets. Mean and standard deviation are shown and only statistically significant differences (* $p < 0.05$) are marked on graphs.

the changes in the ZnO-NPs optical bandgap due to the addition of silver. All coated CF present photocatalytic activity following a pseudo-first-order kinetic equation from the Langmuir-Hinshelwood model (kinetics profile of $\ln(A_t/A_0)$ vs. time in Fig. 3e), indicating that photocatalytic phenomenum involves a high effect from the adsorption step of the dye even in low concentrations [41]. Cotton fabric has photocatalytic activity significantly different from all samples, except for the ZnO(0 ppm) + Ag(500 ppm) sample ($p > 0.05$).

The photocatalytic trapping experiment with the gallic acid (Fig. 3f) indicates that H_2O_2 significantly affects the photocatalytic performance of the CF coated with the nanoparticles because this scavenger drastically reduced the MB photodegradation. All samples present similar photodegradation efficiency under the presence of the gallic acid according to Turkey's tests with a 95% confidence level. HO_2* is the main ROS responsible for the photodegradation activity of the CF coated with ZnO-NPs. This ROS is generated by the decomposition of the H_2O_2 and reaction of H_2O with $^*O_2^-$ in the aqueous media at the surface of the ZnO [16]. The photocatalytic trapping data show that the ROS generation by the Ag/ZnO-NPs involves several complex reactions at the surface of the nanoparticles initiated by complex chemical mechanisms activated by photons that create electron-hole pairs. Moreover, ethanol seems not to be an effective scavenger for electronic holes (h^+) to inhibit the formation of hydroxyl radicals (OH*) by the oxidization of H_2O adsorbed at the surface of the Ag/ZnO hybrid system on the CF [42,43].

Both AgNPs, ZnO-NPs, and Ag/ZnO-NPs (Fig. 4a) enhance the antiviral activity of the CF, reaching a reduction for the infectious SARS-CoV-2 load equal to 31 ± 3% during the first 15 min. This result is indifferent to CF coated by Ag/ZnO-NPs showing superior photodegradation efficiency than the other samples or with AgNPs that display bactericidal activity against *S. aureus*. The amount of SARS-CoV-2 virions is reduced by 15% after 15 min if exposition of the contaminated medium with the uncoated CF. The cycle threshold (Ct) of the SARS-CoV-2 inoculum used in the RT-qPCR test is inferior to 30 (Fig. 4b), suggesting a suitable amount of viral RNA to avoid possible environmental contaminations or failure of the RNA amplification procedure. Moreover, Smyrlaki et al. [44] reported that Ct values do not reduce when SARS-CoV-2 RNA do no fragment, standing stable. Recently, Lista et al. [45] reported that qRT-PCR amplifies the N1 and N2 prime-target genetic sequences of SARS-CoV-2 inactivated or not by heating similarly. At the same time, the Ct values of both viral particles are practically identical. The variance analysis (ANOVA) test with a 95% confidence level indicates no difference in the virus load between the samples due to no significant differences among the number of RNA copies amplified by RT-qPCR for SARS-CoV-2, independently of the regions of the nucleocapsid gene utilized (N1 and N2). The RT-qPCR measurements were performed using the contaminated medium after contact with the coated fabrics.

4. Conclusions

In summary, the Ag/ZnO-coated cotton fabrics present higher photoactivity performance than CF modified only by AgNPs and ZnO-NPs. The silver sonochemical treatment reduces the direct optical bandgap of the ZnO-NPs, whose decrease is accentuated with the increase of the silver content. The content of ZnO and Ag influences the bactericidal activity of the CF. The AgNPs, ZnO-NPs, and hybridous Ag/ZnO-NPs coatings reduce by 20–10% the amount of Delta SARS-CoV-2 virions after 15 min of direct contact with the coated cotton fabrics, bringing on sanitary concerns about the effectiveness of bactericidal multifunctional materials being able to inactivate SARS-CoV-2 variants. The molecular biology data suggest that the AgNPs, ZnO-NPs, and Ag/ZnO hybrid nanoparticles can cause damage to the structural components at the surface of infectious SARS-CoV-2 particles (spike, envelope, and nucleocapsid proteins), failing to affect the viral RNA sufficiently to make its amplification unfeasible by RT-qPCR. The small target genetic sequences of N1 and N2 genes in the inactivated coronavirus may remain intact, and yet suitable to be annealed by the RT-qPCR primer. Then, subsequently, the reverse transcriptase enzyme can assemble the complementary DNA (cDNA) that is amplified by the DNA polymerase in the RT-qPCR assay.

Although international regulatory agencies, such as the United States Environmental Protection Agency (EPA) [46], indicate the usage of disinfectant substances to inactivate SARS-CoV-2 even without direct testing with this coronavirus (e.g., silver), our findings show that AgNPs, ZnO-NPs, and Ag/ZnO nanocomposites may not provide sufficient antimicrobial capacity for CF to ensure a fast inactivation of SARS-CoV-2 virions. The sum of squares for the response surface experimental design (Table 4S) suggests that the content of ZnO-NPs has the main effect on the optical bandgaps of the Ag/ZnO-NPs and the inhibition zone diameter of the bactericidal activity of the CF against *S. aureus*. Finally, the Ag and ZnO concentration factors applied to the CF surface coating do not behave additively but interact over the k photodegradation kinetic parameter. Further studies must be carried out with cotton fabrics coated with higher loadings of AgNPs, ZnONPs, and Ag/ZnO-NPs to evaluate if these bactericidal agents can disrupt the viral RNA of the

Delta and other SARS-CoV-2 variants to an effective viral inactivation.

Funding

This research was funded by Fundação de Amparo à Pesquisa do Estado de São Paulo (2019/16301-6), Conselho Nacional de Desenvolvimento Científico e Tecnológico (305819/2017-8), CAPES-Pandemias (88881.504639/2020-01) and Brazilian National Council of Scientific and Technological Development (CNPq) in partnership with Ministry of Science, Technology, Innovations and Communications (MCTIC), and Brazilian Ministry of Health, Brazil, Secretariat of Science, Technology, Innovation and Strategic Inputs – Decit/SCTIE 07/2020 (Research to cope with COVID-19, its consequences and other severe acute respiratory syndromes – No. 402432/2020-7).

Availability of data and material

Not applicable.

Code availability

Not applicable.

Ethical statement

The study was approved by the Local Ethical Committee of the Faculty of Medicine of ABC (FMABC) (4.427.013, 2020).

Declaration of Competing Interest

The authors declare that they have no known competing financial interests or personal relationships that could have appeared to influence the work reported in this paper.

Acknowledgment

The authors thank the CAPES (Code 001), UFABC nº 48/2020 - REIT (11.01), REVALORES, UFABC, University of São Paulo (USP), Faculdade de Medicina do ABC (FMABC), and Multiuser Central Facilities (UFABC) for the experimental support.

Appendix A. Supplementary data

Supplementary data to this article can be found online at https://doi.org/10.1016/j.jphotobiol.2022.112538.

References

[1] K. Tao, P.L. Tzou, J. Nouhin, R.K. Gupta, T. de Oliveira, S.L. Kosakovsky Pond, D. Fera, R.W. Shafer, The biological and clinical significance of emerging SARS-CoV-2 variants, Nat. Rev. Genet. (2021), 0123456789, https://doi.org/10.1038/s41576-021-00408-x.

[2] Y. Umar, S. Al-Batty, H. Rahman, O. Ashwaq, A. Sarief, Z. Sadique, P.A. Sreekumar, S.K.M. Haque, Polymeric materials as potential inhibitors against SARS-CoV-2, J. Polym. Environ. (2021), https://doi.org/10.1007/s10924-021-02272-6.

[3] F. Magurano, M. Baggieri, A. Marchi, G. Rezza, L. Nicoletti, B. Eleonora, F. Concetta, F. Stefano, K. Maedeh, B. Paola, D. Emilio, G. Silvia, SARS-CoV-2 infection: the environmental endurance of the virus can be influenced by the increase of temperature, Clin. Microbiol. Infect. 27 (289) (2021) e5–289.e7, https://doi.org/10.1016/j.cmi.2020.10.034.

[4] H.A. Aboubakr, T.A. Sharafeldin, S.M. Goyal, Stability of SARS-CoV-2 and other coronaviruses in the environment and on common touch surfaces and the influence of climatic conditions: a review, Transbound. Emerg. Dis. 68 (2021) 296–312, https://doi.org/10.1111/tbed.13707.

[5] E. Orenes-Piñero, F. Baño, D. Navas-Carrillo, A. Moreno-Docón, J.M. Marín, R. Misiego, P. Ramírez, Evidences of SARS-CoV-2 virus air transmission indoors using several untouched surfaces: a pilot study, Sci. Total Environ. 751 (2021), 142317, https://doi.org/10.1016/j.scitotenv.2020.142317.

[6] D.E. Corpet, Why does SARS-CoV-2 survive longer on plastic than on paper? Med. Hypotheses 146 (2021), 110429 https://doi.org/10.1016/j.mehy.2020.110429.

[7] Y. Liu, T. Li, Y. Deng, S. Liu, D. Zhang, H. Li, X. Wang, L. Jia, J. Han, Z. Bei, L. Li, J. Li, Stability of SARS-CoV-2 on environmental surfaces and in human excreta, J. Hosp. Infect. 107 (2021) 105–107, https://doi.org/10.1016/j.jhin.2020.10.021.

[8] J. Virtanen, K. Aaltonen, I. Kivistö, T. Sironen, Survival of SARS-CoV-2 on clothing materials, Adv. Virol. 2021 (2021) 1–5, https://doi.org/10.1155/2021/6623409.

[9] S. Bhattacharjee, C.R. Macintyre, X. Wen, P. Bahl, U. Kumar, A.A. Chughtai, R. Joshi, Nanoparticles incorporated graphene-based durable cotton fabrics, Carbon N. Y. 166 (2020) 148–163, https://doi.org/10.1016/j.carbon.2020.05.029.

[10] W. Yang, B. Zhang, Q. Zhang, L. Wang, B. Song, Y. Ding, C.P. Wong, Adjusting the band structure and defects of ZnO quantum dots via tin doping, RSC Adv. 7 (2017) 11345–11354, https://doi.org/10.1039/C6RA25940E.

[11] Y. Zhang, Y.-H. Wen, J.-C. Zheng, Z.-Z. Zhu, Direct to indirect band gap transition in ultrathin ZnO nanowires under uniaxial compression, Appl. Phys. Lett. 94 (2009), 113114, https://doi.org/10.1063/1.3104852.

[12] A. Sáenz-Trevizo, P. Amézaga-Madrid, P. Pizá-Ruiz, W. Antúnez-Flores, M. Miki-Yoshida, Optical band gap estimation of ZnO Nanorods, Mater. Res. 19 (2016) 33–38, https://doi.org/10.1590/1980-5373-mr-2015-0612.

[13] S.M.H. AL-Jawad, S.H. Sabeeh, A.A. Taha, H.A. Jassim, Studying structural, morphological and optical properties of nanocrystalline ZnO:Ag films prepared by sol–gel method for antimicrobial activity, J. Sol-Gel Sci. Technol. 87 (2018) 362–371, https://doi.org/10.1007/s10971-018-4724-9.

[14] H. Mohd Yusof, R. Mohamad, U.H. Zaidan, N.A. Abdul Rahman, Microbial synthesis of zinc oxide nanoparticles and their potential application as an antimicrobial agent and a feed supplement in animal industry: a review, J. Anim. Sci, Biotechnol. 10 (2019) 57, https://doi.org/10.1186/s40104-019-0368-z.

[15] Q. Li, W. Cao, J. Lei, X. Zhao, T. Hou, B. Fan, D. Chen, L. Zhang, H. Wang, H. Xu, R. Zhang, H. Lu, Synthesis and growth mechanism of ZnO rod-like nanostructures by a microwave-assisted low-temperature aqueous solution route, Cryst. Res. Technol. 49 (2014) 298–302, https://doi.org/10.1002/crat.201300355.

[16] M. Pelaez, N.T. Nolan, S.C. Pillai, M.K. Seery, P. Falaras, A.G. Kontos, P.S. M. Dunlop, J.W.J. Hamilton, J.A. Byrne, K. O'Shea, M.H. Entezari, D.D. Dionysiou, A review on the visible light active titanium dioxide photocatalysts for environmental applications, Appl. Catal. B Environ. 125 (2012) 331–349, https://doi.org/10.1016/j.apcatb.2012.05.036.

[17] A. Sirelkhatim, S. Mahmud, A. Seeni, N.H.M. Kaus, L.C. Ann, S.K.M. Bakhori, H. Hasan, D. Mohamad, Review on zinc oxide nanoparticles: antibacterial activity and toxicity mechanism, Nano-Micro Lett. 7 (2015) 219–242, https://doi.org/10.1007/s40820-015-0040-x.

[18] H. Agarwal, S. Venkat Kumar, S. Rajeshkumar, A review on green synthesis of zinc oxide nanoparticles – an eco-friendly approach, Resour. Technol. 3 (2017) 406–413, https://doi.org/10.1016/j.reffit.2017.03.002.

[19] S. Anees Ahmad, S. Sachi Das, A. Khatoon, M. Tahir Ansari, M. Afzal, M. Saquib Hasnain, A. Kumar Nayak, Bactericidal activity of silver nanoparticles: a mechanistic review, Mater. Sci. Energy Technol. 3 (2020) 756–769, https://doi.org/10.1016/j.mset.2020.09.002.

[20] A. Hassanjani-Roshan, M.R. Vaezi, A. Shokuhfar, Z. Rajabali, Synthesis of iron oxide nanoparticles via sonochemical method and their characterization, Particuology. 9 (2011) 95–99, https://doi.org/10.1016/j.partic.2010.05.013.

[21] N.S.M. Yusof, M. Ashokkumar, Sonochemical synthesis of gold nanoparticles by using high intensity focused ultrasound, ChemPhysChem. 16 (2015) 775–781, https://doi.org/10.1002/cphc.201402697.

[22] M. Ali Dheyab, A. Abdul Aziz, M.S. Jameel, P. Moradi Khaniabadi, B. Mehrdel, Sonochemical-assisted synthesis of highly stable gold nanoparticles catalyst for decoloration of methylene blue dye, Inorg. Chem. Commun. 127 (2021), 108551, https://doi.org/10.1016/j.inoche.2021.108551.

[23] N. Silva, S. Ramírez, I. Díaz, A. Garcia, N. Hassan, Easy, quick, and reproducible Sonochemical synthesis of CuO nanoparticles, Materials (Basel). 12 (2019) 804, https://doi.org/10.3390/ma12050804.

[24] P. Petkova, A. Francesko, M.M. Fernandes, E. Mendoza, I. Perelshtein, A. Gedanken, T. Tzanov, Sonochemical coating of textiles with hybrid ZnO/chitosan antimicrobial nanoparticles, ACS Appl. Mater. Interfaces 6 (2014) 1164–1172, https://doi.org/10.1021/am404852d.

[25] D.J. da Silva, A.G. Souza, G. da S. Ferreira, A. Duran, A.D. Cabral, F.L.A. Fonseca, R.F. Bueno, D.S. Rosa, Cotton fabrics decorated with antimicrobial Ag-coated TiO2 nanoparticles are unable to fully and rapidly eradicate SARS-CoV-2, ACS Appl, Nanostruct. Mater. (2021), https://doi.org/10.1021/acsanm.1c03492 acsanm.1c03492.

[26] R.R. Ferreira, A.G. Souza, L.L. Nunes, N. Shahi, V.K. Rangari, D. Dos S. Rosa, Use of ball mill to prepare nanocellulose from eucalyptus biomass: challenges and process optimization by combined method, Mater. Today Commun. 22 (2020), 100755, https://doi.org/10.1016/j.mtcomm.2019.100755.

[27] J. Kavuličová, A. Mražíková, O. Velgosová, D. Ivánová, M. Kubovčíková, Stability of synthesized silver nanoparticles in citrate and mixed gelatin/citrate solution, Acta Polytech. 58 (2018) 104, https://doi.org/10.14311/AP.2018.58.0104.

[28] M. Weiße, C. Schmidt, A. Abramova, Y. Voitov, M. Stelter, P. Braeutigam, Sonochemical coating: effect of energy input and distance on the functionalization of textiles with TiO_2 and ZnO-nanoparticles, Ultrason. Sonochem. 60 (2020), 104801, https://doi.org/10.1016/j.ultsonch.2019.104801.

[29] S. Li, J.L. Li, Q. Jiang, G.W. Yang, Electrical field induced direct-to-indirect bandgap transition in ZnO nanowires, J. Appl. Phys. 108 (2010), 024302, https://doi.org/10.1063/1.3462407.

[30] A.A. El-Bindary, S.M. El-Marsafy, A.A. El-Maddah, Enhancement of the photocatalytic activity of ZnO nanoparticles by silver doping for the degradation of AY99 contaminants, J. Mol. Struct. 1191 (2019) 76–84, https://doi.org/10.1016/j.molstruc.2019.04.064.

[31] Y. Zhang, Y.-H. Wen, J.-C. Zheng, Z.-Z. Zhu, Strain-induced structural and direct-to-indirect band gap transition in ZnO nanotubes, Phys. Lett. A 374 (2010) 2846–2849, https://doi.org/10.1016/j.physleta.2010.04.069.
[32] D.J. da Silva, R.F. da Silva Barbosa, A.G. de Souza, R.R. Ferreira, P.H. Camani, I. L. Nantes-Cardoso, D.S. Rosa, Bactericidal activity of cotton fabrics functionalized by ZnO and cu via microwave, Cellulose. 28 (2021) 8153–8175, https://doi.org/10.1007/s10570-021-03990-9.
[33] I. Ahmad, C. Kan, Z. Yao, Photoactive cotton fabric for UV protection and self-cleaning, RSC Adv. 9 (2019) 18106–18114, https://doi.org/10.1039/C9RA02023C.
[34] K.V.T. Nguyen, F.S. Ameer, J.N. Anker, J.L. Brumaghim, H.C. Minh, Reactive oxygen species generation by copper(II) oxide nanoparticles determined by DNA damage assays and EPR spectroscopy, Nanotoxicology. 11 (2017) 278–288, https://doi.org/10.1080/17435390.2017.1293750.Reactive.
[35] J. Liu, J. Wang, S. Lee, R. Wen, Copper-caused oxidative stress triggers the activation of antioxidant enzymes via ZmMPK3 in maize leaves, PLoS One 13 (2018), e0203612, https://doi.org/10.1371/journal.pone.0203612.
[36] J. Manna, S. Goswami, N. Shilpa, N. Sahu, R.K. Rana, Biomimetic method to assemble nanostructured Ag@ZnO on cotton fabrics: application as self-cleaning flexible materials with visible-light Photocatalysis and antibacterial activities, ACS Appl. Mater. Interfaces 7 (2015) 8076–8082, https://doi.org/10.1021/acsami.5b00633.
[37] S. Adhikari, A. Banerjee, N.K.R. Eswar, D. Sarkar, G. Madras, Photocatalytic inactivation of *E. coli* by ZnO-Ag nanoparticles under solar radiation, RSC Adv. 5 (2015) 51067–51077, https://doi.org/10.1039/c5ra06406f.
[38] S. Wang, J. Wu, H. Yang, X. Liu, Q. Huang, Z. Lu, Antibacterial activity and mechanism of Ag/ZnO nanocomposite against anaerobic oral pathogen Streptococcus mutans, J. Mater. Sci. Mater. Med. 28 (2017) 23, https://doi.org/10.1007/s10856-016-5837-8.
[39] O. Akhavan, Lasting antibacterial activities of Ag–TiO_2/Ag/a-TiO2 nanocomposite thin film photocatalysts under solar light irradiation, J. Colloid Interface Sci. 336 (2009) 117–124, https://doi.org/10.1016/j.jcis.2009.03.018.
[40] H. Deng, H. He, S. Sun, X. Zhu, D. Zhou, F. Han, B. Huang, X. Pan, Photocatalytic degradation of dye by Ag/TiO_2 nanoparticles prepared with different sol–gel crystallization in the presence of effluent organic matter, Environ. Sci. Pollut. Res. 26 (2019) 35900–35912, https://doi.org/10.1007/s11356-019-06728-0.
[41] B.C.B. Salgado, A. Valentini, Evaluation of the photocatalytic activity of SiO_2@TiO_2 hybrid spheres in the degradation of methylene blue and hydroxylation of benzene: kinetic and mechanistic study, Brazilian, J. Chem. Eng. 36 (2019) 1501–1518, https://doi.org/10.1590/0104-6632.20190364s20190139.
[42] X.H. Yang, H.T. Fu, X.C. Wang, J.L. Yang, X.C. Jiang, A.B. Yu, Synthesis of silver-titanium dioxide nanocomposites for antimicrobial applications, J. Nanopart. Res. 16 (2014) 2526, https://doi.org/10.1007/s11051-014-2526-8.
[43] Z. Li, Q. Zhang, X. Liu, L. Wu, H. Hu, Y. Zhao, One-step mechanochemical synthesis of plasmonic Ag/Zn–Al LDH with excellent photocatalytic activity, J. Mater. Sci. 53 (2018) 12795–12806, https://doi.org/10.1007/s10853-018-2537-4.
[44] I. Smyrlaki, M. Ekman, A. Lentini, N. Rufino de Sousa, N. Papanicolaou, M. Vondracek, J. Aarum, H. Safari, S. Muradrasoli, A.G. Rothfuchs, J. Albert, B. Högberg, B. Reinius, Massive and rapid COVID-19 testing is feasible by extraction-free SARS-CoV-2 RT-PCR, Nat. Commun. 11 (2020) 4812, https://doi.org/10.1038/s41467-020-18611-5.
[45] M.J. Lista, P.M. Matos, T.J.A. Maguire, K. Poulton, E. Ortiz-Zapater, R. Page, H. Sertkaya, A.M. Ortega-Prieto, E. Scourfield, A.M. O'Byrne, C. Bouton, R. E. Dickenson, M. Ficarelli, J.M. Jimenez-Guardeño, M. Howard, G. Betancor, R. P. Galao, S. Pickering, A.W. Signell, H. Wilson, P. Cliff, M.T. Kia Ik, A. Patel, E. MacMahon, E. Cunningham, K. Doores, M. Agromayor, J. Martin-Serrano, E. Perucha, H.E. Mischo, M. Shankar-Hari, R. Batra, J. Edgeworth, M. Zuckerman, M.H. Malim, S. Neil, R.T. Martinez-Nunez, Resilient SARS-CoV-2 diagnostics workflows including viral heat inactivation, PLoS One 16 (2021), e0256813, https://doi.org/10.1371/journal.pone.0256813.
[46] U.S.E.P.A. EPA, List N: Disinfectants for coronavirus (COVID-19), list N disinfect, Coronavirus. 2 (2020) 1–2. https://cfpub.epa.gov/wizards/disinfectants/.